CHAPTER 2

FUNDAMENTAL THEORY AND MULTIMODE ANALYSIS OF DIELECTRIC LOADED GYRO-TWT*

**Part of this work has been published as:

Akash and M. Thottappan, "Stability and Multimode Simulation Studies of W-Band Uniformly Dielectric-Loaded Gyrotron Traveling-Wave Tube Amplifier," *IEEE Trans. Electron Devices*, vol. 66, no. 12, pp. 5305-5312, Dec. 2019 (10.1109/TED.2019.2944487).

2.1. Introduction

This chapter discusses the solution of Maxwell's equations to study the wave propagation in the uniform and periodic lossy dielectric loaded waveguide. The basic theory of lossy dielectric loaded cylindrical waveguide is studied first to address the dispersion relation in the gyro-TWT operation. Since, the lossy waveguide interaction system has been proved effective to suppress various instabilities; the full-wave interaction analysis of lossy dielectric loaded waveguide structure for gyro-TWT using linear and nonlinear theories have been reviewed [Du and Liu (2010), (2010)]. Nonlinear analyses of gyro-TWT reported so far have considered only single waveguide mode interaction with the electron beam [Sprangle and Drobot (1977), Chu (2004), Wang *et al*. (1992)]. The single-mode theory of the distributed lossy waveguide was introduced by Chu *et al.* [Chu *et al*. (1999)]. Using the single-mode theory, one can preliminarily select the structural and electrical parameters of the system to analyze the growth of the operating mode. However, to analyze the backward wave oscillation and their effect on the growth of the operating as well as competing modes, one must consider multiple modes interaction with the beam at the same time. In this chapter, a multimode steady-state nonlinear analysis of gyro-TWT is presented to analyze the mutual effects among more than one waveguide modes, including the operating mode and backward wave oscillation modes for a uniform dielectric-loaded (UDL) waveguide and the periodic dielectric loaded (PDL) waveguide. The motion of electrons is affected by both the operating mode and backward wave oscillation modes. With the help of multimode analysis, one can discuss the effect of backward wave oscillation modes on the operating mode, which cannot be performed through the single-mode theory. This section reviews the theory of dielectric-loaded waveguide which provides theoretical foundation for studying the waveguide propagation characteristics.

2.2. Theory of Dielectric Waveguides

The development of gyro-TWT amplifier including various types of interaction waveguide structures such as dielectric loading, photonic band gap structures, confocal waveguide, helically corrugated waveguide, etc. have been experimentally and theoretically reported. While employing a certain kind of structure as RF interaction circuit, the primary motive is generally remained to suppress the various oscillations and get the zero-drive stability [Du and Liu (2014)]. Among various kind of interaction waveguide structure, the lossy dielectric loaded interaction circuit has been proved as operation mode control method that effectively suppresses these oscillations by providing the heavy attenuation to the oscillating modes. The lossy dielectric controls the propagation characteristic of the operating as well as competing modes that directly influence the beam-particle interaction. This chapter reviews the theory of dielectric-loaded waveguide which provides theoretical foundation of the propagation characteristic of the RF beam in the lossy dielectric waveguides.

2.2.1. Theory of Uniform Dielectric Waveguide

Figure 2.1 depicts the longitudinal and transverse view of uniform dielectric loaded cylindrical waveguide. The dielectric loaded waveguide is divided into two regions, Region I, is the empty waveguide region filled with vacuum and Region 2, is the lossy region filled with the lossy dielectric layer. According to the solution of Maxwell's equations, the electric and magnetic field component in the vacuum filled and dielectric filled regions of a dielectric loaded cylindrical waveguide system can be separately expressed as [Harrington (2001)],

Vacuum Region

$$E_z = -jA(z)\chi J_m(k_{\perp 1} r)\, e^{j(\omega t - m\varphi)} \tag{2.1a}$$

$$H_z = A(z) J_m(k_{\perp 1} r)\, e^{j(\omega t - m\varphi)} \tag{2.1b}$$

$$E_r = \left[-A(z)\frac{m}{r}\frac{\omega\mu_1}{k_{\perp 1}^2} J_n(k_{\perp 1} r) - jA'(z)\frac{1}{k_{\perp 1}}\chi J'_m(k_{\perp 1} r) \right] e^{j(\omega t - m\varphi)} \tag{2.1c}$$

$$H_r = \left[-A'(z)\frac{1}{k_{\perp 1}} J'_m(k_{\perp 1} r) - jA(z)\frac{m}{r}\frac{\omega\varepsilon_1}{k_{\perp 1}^2}\chi J_m(k_{\perp 1} r) \right] e^{j(\omega t - m\varphi)} \tag{2.1d}$$

$$E_\varphi = \left[-jA(z)\frac{\omega\mu_1}{k_{\perp 1}^2} J'_m(k_{\perp 1} r) - A'(z)\frac{m}{r}\frac{1}{k_{\perp 1}}\chi J_m(k_{\perp 1} r) \right] e^{j(\omega t - m\varphi)} \tag{2.1e}$$

$$H_\varphi = \left[-jA'(z)\frac{m}{k_{\perp 1}^2 r} J_m(k_{\perp 1} r) - A(z)\frac{\omega\varepsilon_1}{k_{\perp 1}}\chi J_m(k_{\perp 1} r) \right] e^{j(\omega t - m\varphi)} \tag{2.1f}$$

Dielectric Region

$$E_z = -jA(z)\left[\tilde{\alpha} J_m(k_{\perp 2} r) + \tilde{\beta} N_m(k_{\perp 2} r) \right] e^{j(\omega t - m\varphi)} \tag{2.2a}$$

$$H_z = A(z)\left[\alpha J_m(k_{\perp 2} r) + \beta N_m(k_{\perp 2} r) \right] e^{j(\omega t - m\varphi)} \tag{2.2b}$$

$$E_r = \begin{bmatrix} -A(z)\frac{m}{r}\frac{\omega\mu_2}{k_{\perp 2}^2}\left(\alpha J_m(k_{\perp 2} r) + \beta N_m(k_{\perp 2} r) \right) \\ -jA'(z)\frac{1}{k_{\perp 2}}\left(\tilde{\alpha} J'_m(k_{\perp 2} r) + \tilde{\beta} N'_m(k_{\perp 2} r) \right) \end{bmatrix} e^{j(\omega t - m\varphi)} \tag{2.2c}$$

$$H_r = \begin{bmatrix} A'(z)\frac{1}{k_{\perp 2}}\left(\alpha J'_m(k_{\perp 2} r) + \beta N'_m(k_{\perp 2} r) \right) \\ -jA(z)\frac{m}{r}\frac{\omega\varepsilon_2}{k_{\perp 2}^2}\left(\tilde{\alpha} J_m(k_{\perp 2} r) + \tilde{\beta} N_m(k_{\perp 2} r) \right) \end{bmatrix} e^{j(\omega t - m\varphi)} \tag{2.2d}$$

$$E_\varphi = \begin{bmatrix} -jA(z)\frac{\omega\mu_2}{k_{\perp 2}}\left(\alpha J'_m(k_{\perp 2} r) + \beta N'_m(k_{\perp 2} r) \right) \\ -jA'(z)\frac{m}{r}\frac{1}{k_{\perp 2}^2}\left(\tilde{\alpha} J_m(k_{\perp 2} r) + \tilde{\beta} N_m(k_{\perp 2} r) \right) \end{bmatrix} e^{j(\omega t - m\varphi)} \tag{2.2e}$$

$$H_\varphi = \begin{bmatrix} -jA'(z)\frac{m}{r}\frac{1}{k_{\perp 2}^2}\left(\alpha J_m(k_{\perp 2} r) + \beta N_m(k_{\perp 2} r) \right) \\ -A(z)\frac{\omega\varepsilon_2}{k_{\perp 2}}\left(\tilde{\alpha} J'_m(k_{\perp 2} r) + \tilde{\beta} N'_m(k_{\perp 2} r) \right) \end{bmatrix} e^{j(\omega t - m\varphi)} \tag{2.2f}$$

where, $A(z)$ is the axial field amplitude and α, β, $\tilde{\alpha}$, $\tilde{\beta}$ are arbitrary constants. The permittivity and permeability constants of vacuum and dielectric regions are $\varepsilon_1 = \varepsilon_0$, $\mu_1 = \mu_0$, $\varepsilon_2 = \varepsilon_0 \varepsilon_r$, and $\mu_2 = \mu_0 \mu_r$ respectively. The functions J_n and N_n are the Bessel functions of first and second kind. The boundary conditions for the fields are continuous

tangential field components at the interface $r = r_w$ and vanishing tangential electric field at the perfect conductor $r = r_w + \Delta r$,:

At the surface $r = r_w$,

$$E_\varphi^I = E_\varphi^{II} \text{ and } H_z^I = H_z^{II}; \qquad \text{for } 0 \le z < L_1,$$

$$E_\varphi^I = 0; \qquad \text{for } L_1 \le z < L_1 + L_2.$$

At the surface $r = r_w + \Delta r$,

$$E_\varphi^{II} = 0; \qquad \text{for } 0 < z < L_1$$

With these boundary conditions, the system of equations (2.1a - 2.1f) and (2.2a - 2.2f) can be recast into the dispersion relation [Du *et al*. (2014)]

$$\left[\frac{1}{k_{\perp 1}}\frac{J_m'(k_{\perp 1}r_\omega)}{J_m(k_{\perp 1}r_\omega)} - \frac{\mu_2}{\mu_1}\frac{P'(k_{\perp 1}(r_\omega)}{P(k_{\perp 2}r_\omega)}\right] \times \left[\frac{1}{k_{\perp 1}}\frac{J_m'(k_{\perp 1}r_\omega)}{J_m(k_{\perp 1}r_\omega)} - \frac{\varepsilon_2}{\varepsilon_1}\frac{Q'(k_{\perp 1}r_\omega)}{Q(k_{\perp 2}r_\omega)}\right] - \frac{1}{\mu_1\varepsilon_1}\left(\frac{k_z m}{\omega R_\omega}\right)^2 \left[\frac{1}{k_{\perp 1}^2} - \frac{1}{k_{\perp 2}^2}\right]^2 = 0 \tag{2.3}$$

where,

$$\begin{aligned} P(x) &= J_m(x)\,N_m'\left\{k_{\perp 2}(r_\omega + \nabla r)\right\} - Y_m(x)J_m'\left\{k_{\perp 2}(r_\omega + \nabla r)\right\}, \\ P'(x) &= J_m'(x)\,N_m'\left\{k_{\perp 2}(r_\omega + \nabla r)\right\} - Y_m'(x)J_m'\left\{k_{\perp 2}(r_\omega + \nabla r)\right\}, \\ Q(x) &= J_m(x)\,N_m\left\{k_{\perp 2}(r_\omega + \nabla r)\right\} - Y_m(x)J_m\left\{k_{\perp 2}(r_\omega + \nabla r)\right\}, \\ Q'(x) &= J_m'(x)\,N_m\left\{k_{\perp 2}(r_\omega + \nabla r)\right\} - Y_m'(x)J_m\left\{k_{\perp 2}(r_\omega + \nabla r)\right\}, \end{aligned} \tag{2.4}$$

For m = 0 and $k_z = 0$, the equation (2.3) splits into TE and TM modes fields and can be expressed as,

$$\left[\frac{1}{k_{\perp \mathrm{I}}}\frac{J_m'(k_{\perp \mathrm{I}}r_\omega)}{J_m(k_{\perp \mathrm{I}}r_\omega)} - \frac{1}{k_{\perp \mathrm{II}}}\frac{\mu_{II}}{\mu_I}\frac{P'(k_{\perp \mathrm{II}}r_\omega)}{P(k_{\perp \mathrm{II}}r_\omega)}\right] = 0 \ , \quad \text{for } TE \text{ mode} \tag{2.5}$$

$$\left[\frac{1}{k_{\perp \mathrm{I}}}\frac{J_m'(k_{\perp \mathrm{I}}r_\omega)}{J_m(k_{\perp \mathrm{I}}r_\omega)} - \frac{1}{k_{\perp \mathrm{II}}}\frac{\varepsilon_{II}}{\varepsilon_I}\frac{Q'(k_{\perp \mathrm{II}}r_\omega)}{Q(k_{\perp \mathrm{II}}r_\omega)}\right] = 0 \ , \quad \text{for } TM \text{ mode} \tag{2.6}$$

For $k_z \neq 0$ and $m \neq 0$, the solution of equation (2.3) has complex field distribution *i.e.*, hybrid $HE_{m,n}$ or $EH_{m,n}$ modes. The transcendental equation (2.3) is solved along

with the following dispersion relations,

$$k_{\perp 1}^2 + k_z^2 = k^2 = \omega^2 \varepsilon_1 \mu_1, \quad \text{(Region I)} \tag{2.7}$$

$$k_{\perp 2}^2 + k_z^2 = k^2 = \omega^2 \varepsilon_2 \mu_2, \quad \text{(Region II)} \tag{2.8}$$

The solution of the dispersion equation for real ω is having a complex wave number ($k_r + jk_i$) with $|k_i| >> k_r$ near the cut-off region. Therefore, the dispersion curve of modes is discontinuous near the cut-off region due to high attenuation by the lossy dielectric.

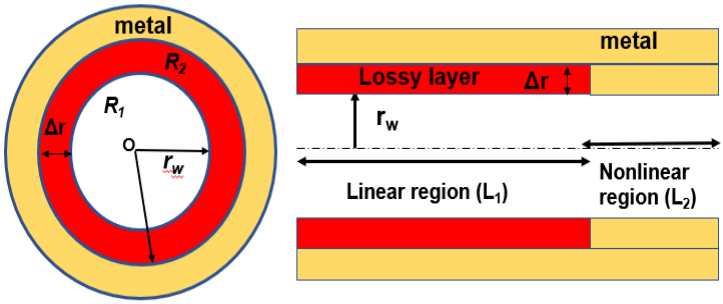

Figure 2.1. Schematic of UDL RF interaction structure for W-band gyro-TWT (a) transverse view and (b) longitudinal view.

2.2.2. Theory of Periodic Dielectric Loaded (PDL) Waveguide

The cross-section of PDL waveguide is divided into two regions namely: (i) vacuum region (R_1), and (ii) dielectric region (R_2). In region R_1, the wave is propagating one, and according to the Floquet's theorem, the axial magnetic field in R_1 is expressed as a sum of Bloch harmonics [Tigelis *et al.* (1998), Kesari *et al.* (2011)].

$$E_z^1 = \sum_{n=-\infty}^{+\infty} A_n^1 J_m\left(h_n^1 r\right) \mathrm{e}^{j(\omega\varphi - k_n z)} \qquad r < a \tag{2.9}$$

$$H_z^1 = \sum_{n=-\infty}^{+\infty} B_n^1 J_m\left(h_n^1 r\right) \mathrm{e}^{j(\omega\varphi - k_n z)} \qquad r < a \tag{2.10}$$

In the periodic system, the propagation constant is $k_n = k + n\,(2\pi / L)$, where m and n indicate the order numbers of the Bessel Function and the Bloch harmonic, respectively. A_n^1 and B_n^2 are the unknown coefficients of field's amplitude and $\left(h_n^1\right)^2 = (\omega / c)^2 - k_n^2$,

represent the inverse characteristic length in region R_1. The axial component of magnetic field in dielectric region R_2 corresponds to standing eigenwaves, which are represented by Fourier series [Tigelis *et al.* (1998)],

$$E_z^2 = \sum_{l=1}^{+\infty} A_l^2 Z_m\left(h_l^2 r\right) \mathrm{e}^{j(\omega t)} \cos\left(l\pi z / b\right) \qquad (a < r < b,\ nL < z < b + nL) \tag{2.11}$$

$$H_z^2 = \sum_{l=1}^{+\infty} B_l^2 Z_m\left(h_l^2 r\right) \mathrm{e}^{j(\omega t)} \sin\left(l\pi z / b\right) \qquad (a < r < b,\ nL < z < b + nL) \tag{2.12}$$

where, $\left(h_n^2\right)^2 = \varepsilon_r \left(\omega / c\right)^2 - \left(l\pi / b\right)^2$ represent the inverse characteristic length in region R_2. $Z_m\left(h_l^2 r\right) = J_m\left(h_l^2 r\right) Y_0'\left(h_l^2 r_w\right) - J_m'\left(h_l^2 r\right) Y_0\left(h_l^2 r_w\right)$ is combined function of modified Bessel and Neumann functions. In order to characterize the transverse field equation for the present periodic dielectric waveguide, relevant boundary conditions are needed to be incorporated. The tangential electric and magnetic fields must be continuous at the interface between region (R_1) and region (R_2) at $r = r_{w,}$

$$E_\varphi^1 = E_\varphi^2, \text{ and } H_z^1 = H_z^2 \qquad \text{for } 0 \le z < b \tag{2.13}$$

The tangential electric field should vanish at the interface between vacuum and perfect conductor at $r = r_w$,

$$E_\varphi^1 = 0 \qquad \text{for } \ b + nL \le z < (n+1)\,L \tag{2.14}$$

The tangential electric field should also vanish for the interface between dielectric and perfect conductor at $r = r_w + d$,

$$E_\varphi^2 = 0 \qquad \text{for} \qquad 0 \le z < b \tag{2.15}$$

As each period of periodic dielectric-loaded waveguide contains two sections, namely, a dielectric section and a copper region. The modes will have complex field distribution. The transverse field distribution of TE_{11}, TE_{21}, TE_{01}, and TE_{02} mode in the dielectric section, maps to the modes that in the uniform DL waveguide *i.e.*, HE_{12}^d, HE_{22}^d, TE_{02}^d,

and TE_{04}^{d}. While in the copper region, modes are similar to that in the conventional copper waveguide. Due to such a mapping relationship, four modes namely, ~TE_{11}, ~TE_{21}, ~TE_{01}, and ~TE_{02}, are used for the mode's nomenclature in the periodic dielectric waveguide [Du *et al.* (2009)].

2.3. Theory of CRM interaction in lossy Dielectric loaded Gyro-TWT

The theoretical modal for CRM interaction in gyro-TWT system developed in this section is valid with limitations. It is only valid for ECM system of longitudinal uniformity and considering only TE mode or TE mode-like hybrid mode. Three basic assumptions are made [Chu (2004), Wang *et al.* (1992)]:

Single Mode Interaction: The electron beam interacts with a single mode and reaches a steady state in frequency domain.

Undisturbed Mode Distribution: The wave mode in the interaction circuit maintains the same transverse distribution as it is in an electron-free waveguide. The beam-wave interaction influences the wave amplitude only.

Omitting the Space Charge Effect: The space charge from the electron beam imposes no influence on the beam-wave interaction.

A transverse cross sectional of a general CRM interaction waveguide system is shown in Figure 1. The waveguide system is parted into two regions. The region 1 is the vacuum region containing electron beam, while remaining complicate region is region 2. The region 2 contains the disturbance structure (*e.g.,* lossy layer) introduce to control the waveguide mode. For a waveguide system, the major field components for a TE mode or a hybrid HE mode, most energy of which is carried by TE mode components [Calame et *al.*, (2002), Du et al. (2009)].

Using the Maxwell's equation and considering the distributed current density source $J_{\perp}$,

the wave equation can be expressed as,

$$\left(\frac{d^2}{dz^2}+k_z^2\right)\vec{E}_\perp = j\omega\mu\vec{J}_\perp \tag{2.16}$$

Now, operating with $\left(\frac{\omega}{2\pi}\right)\int_0^{2\pi/\omega} dt \iint_{R_1+R_2} E_\perp^* / A^*(z)\, dS$ on the both sides of the above equation, the beam-wave interaction equation can be expressed as,

$$\left(\frac{d^2}{dz^2}+k_z^2\right)A(z)G = \left(\frac{\omega}{2\pi}\right)\int_0^{2\pi/\omega} \iint_{R_1+R_2} j\omega\mu\vec{J}_\perp . \frac{E_{\perp 1}^*}{A^*(z)}\, dS\, dt \tag{2.17}$$

The above equation is the field exciting equations for linear and self-consistent nonlinear theories, where, R_1 and R_2 indicate the transverse areas of Region 1 and Region 2, respectively, and G is the geometry factor.

2.3.1. Linear theory of lossy Dielectric Loaded Gyro-TWT

In general, the modes in a uniform dielectric-loaded waveguide are hybrid ones HE_{mn} or EH_{mn}. In a gyro-TWT application, properly designed dielectric-loaded waveguide conveys an operation mode with a TE mode like energy distribution, and this hybrid mode is quite similar to a pure TE mode in a cylindrical waveguide [Garven *et al.* (2002), Lee *et al.* (1986), Du (2009)]. According to research experience, an CRM system only considers TE mode components could evaluate the interaction performance with reasonable accuracy [Du and Liu (2009)]. Substituting the field expressions of the TE component of a hybrid mode in dielectric waveguide into Eq. (2.17)

$$\left(\frac{d^2}{dz^2}+k_z^2\right)A(z)G_{mn} = \frac{-1}{j\omega\mu A^*(z)}\left(\frac{\omega}{2\pi}\right)\int_0^{2\pi/\omega}\int_0^{r_w}\int_0^{2\pi} (\vec{J}_\theta . \vec{E}_\theta^*)\, r\, dr\, d\phi\, dt. \tag{2.18}$$

where, $\vec{J}_\theta$ is the disturbing current, $\vec{E}_\theta$ is field expression in the guiding center coordinate of the electron beam, the geometry factor is $G_{mn} = G_1 + G_2$, and the constants G_1 and G_2 are given as,

$$G_1 = \pi r_w^2 \left(1 - \frac{m^2}{k_t^2 r_w^2}\right) J_m^2 \left(k_t r_w\right) \tag{2.19}$$

$$G_2 = \frac{2\pi}{k_{tl}^2} \int_{r_w}^{r_w+t} \left\{ \begin{array}{l} \left|\alpha J_m'(k_{tl} r) + \beta N_{mp}^{'}(k_{tl} r)\right|^2 \\ + \left|\dfrac{m}{k_{tl} r}[\alpha J_m(k_{tl} r) + \beta N_{mp}(k_{tl} r)]\right|^2 \end{array} \right\} r\, dr \tag{2.20}$$

when the dielectric layer is eliminated, the geometry factor becomes $G_{mn} = G_1$, and returns to a beam-wave interaction equation of a cylindrical waveguide-based CRM system [Chu *et al.* (1999)]. Linearizing the relativistic Vlasov's equation and after Laplace transformed, the dispersion relation and field amplitude of the dielectric-loaded CRM system can be expressed as [Du and Liu (2010), Kou *et al.* (1992)] ,

$$D(\omega, k_z) = (k_{zc}^2 - k_z^2)\, G_{mn} - \widehat{S}_1(k_z) = 0 \tag{2.21}$$

$$A(z) = \sum_{i=1}^{4} \left[F(0) \frac{\hat{S}_0(k_{zi}) - j k_{zi} G_{mn}}{j D'(k_{zi})} + F'(0) \frac{G_{mn}}{j D'(k_{zi})} \right] e^{-j k_{zi} z} \tag{2.22}$$

where, k_{zc} is the cold propagating constant of the waveguide, and constants $\widehat{S}_1(k_z)$ and $\hat{S}_0(k_{zi})$ are respectively.

$$\begin{aligned} \widehat{S}_1(k_z) = {} & \frac{4\pi^2 e^2 \mu_1}{k_{\perp 1}^2 m_0} \int_0^{r_w} r_c\, dr_c \int_0^{\infty} p_\perp\, dp_\perp \int_0^{\infty} dp_z \frac{f_0}{\gamma} \\ & \times \sum_{s=-\infty}^{\infty} \left[\frac{-\beta_t^2 (\omega^2 - k_z^2 c^2) H_{sm}}{(\omega - s\Omega - k_z v_z)^2} + \frac{(\omega - k_z v_z) T_{sm} - k_\perp v_t U_{sm}}{(\omega - s\Omega - k_z v_z)} \right] \end{aligned} \tag{2.23}$$

$$\begin{aligned} \widehat{S}_0(k_z) = {} & j \frac{4\pi^2 e^2 \mu_1}{k_{\perp 1}^2 m_0} \int_0^{r_w} r_c\, dr_c \int_0^{\infty} p_\perp\, dp_\perp \int_0^{\infty} dp_z \frac{f_0}{\gamma} \\ & \times \sum_{s=-\infty}^{\infty} \left[\frac{-k_z v_t^2 H_{sm}}{(\omega - s\Omega - k_z v_z)^2} + \frac{v_z T_{sm}}{(\omega - s\Omega - k_z v_z)} \right] \end{aligned} \tag{2.24}$$

where,

$$H_{sm}(x, y) = \left| J_s'(x) J_{m-s}(y) \right|^2 \tag{2.25}$$

$$T_{sm}(x,y) = 2H_{sm} + 2\,\mathrm{Re}[xJ'_s(x)J''_s(x)]\left|J_{m-s}(y)\right|^2 - xJ'^{*}_s(x)J_s(x) \times\left[\tfrac{1}{y}J^{*}_{m-s}(y)J'_{m-s}(y) + \tfrac{y^*}{y}\left|J'_{m-s}(y)\right|^2 + J^{*}_{m-s}(y)J''_{m-s}(y)\right] \tag{2.26}$$

$$Usm(x,y) = (-\tfrac{x}{2})J'^{*}_s(x)\left\{\begin{array}{l} J_{s+1}(x)\left[\tfrac{y^*}{y}\left|J_{m-s-1}(y)\right|^2 - \left|J_{m-s}(y)\right|^2\right] \\ +J_{s-1}(x)\left[\tfrac{y^*}{y}\left|J_{m-s+1}(y)\right|^2 - \left|J_{m-s}(y)\right|^2\right] \end{array}\right\} \tag{2.27}$$

other variables are $x = k_{\perp 1} r_L$ and $y = k_{\perp 1} r_c$. The linear theory takes into consideration the influence of the dielectric layer loaded to the propagation characteristics and field distribution and is capable of efficiently analyzing the CRM interaction.

2.3.2. Nonlinear theory of lossy Dielectric Loaded Gyro-TWT

Similar to the linear theory, the nonlinear theory of the dielectric-loaded waveguide considers a pure TE mode or the TE mode component of a hybrid mode. Substituting the field components into (2.30), it is obtained as follows:

$$\left(\frac{\partial^2}{\partial z^2} + k_z^2\right)A_p(z) = \left(\frac{-2\left|I_0\right|}{G_{mn}}\right)\sum_{i=1}^{N} W_i \frac{\vec{\beta}_i}{\beta_{zi}}\left[\frac{1}{k_{\perp 1}}\sum_{s=-\infty}^{\infty} J'_s(k_{\perp 1}r_{Li})J_{m-s}(k_{\perp 1}r_{ci})e^{j\Lambda_i}\right]^* \tag{2.28}$$

where, the beam current density is assumed to be

$$\vec{J} = -\frac{2\pi\left|I_0\right|}{\omega}\sum_{i=1}^{N} W_i \frac{1}{r_i}\,\delta(r-r_i)\,\delta(\varphi-\varphi_i)\,\delta(t-t_i)\,\frac{\vec{\beta}_i}{\beta_{zi}} \tag{2.29}$$

where, the phase distribution is $\Lambda_i = \omega t_i - s\,\theta_i - (m-s)\,\phi_{ci}$ and the weight factor of macro particle follows $\sum_{i=1}^{N} W_i = 1$.

2.4. Nonlinear Multimode Theory of Dielectric Loaded Gyro-TWT

The steady state nonlinear multimode theory discussed here for the two types of distributed loss-loaded waveguide modes, (1) UDL waveguide and (2) PDL waveguide. The beam wave interaction circuit of gyro-TWT mainly divided into two sections (i) loaded linear section and (ii) unloaded nonlinear section. In the UDL waveguide model,

the linear section of the interaction circuit is uniform loaded waveguide with lossy material. For the PDL waveguide model, the linear section has periodic arrangement of alternate lossy materials and metal rings. For both the structures, the radius of the waveguide is r_w, and the thickness of the lossy material is Δr. The PDL structure has a period length of L and a lossy material length of b within each period. Considering that more than one mode simultaneously interacts with the electrons in the cylindrical waveguide, N field-evolving equations (N is the number considered the modes in the waveguide) and six electron-evolving equations are deduced from Maxwell's equations and Lorentz's equation for the multimode steady state theory. Various assumptions are used in the abovementioned discussion, which typically appear as follows in the classic single-mode theory [Du and Liu (2010)]; (i) the transverse field distribution of electromagnetic modes is not affected by the electrons in the cylindrical waveguide, and the variation of the field amplitude only takes place in the axial direction and (ii) space charge force among electrons is not considered.

2.4.1. Wave Dynamics in UDL Waveguide Linear Section

The loss is uniformly distributed along the entire length (L_1) of the linear section. Assuming that only transverse electric (*TE*) modes (E_z = 0) are propagating in the RF interaction circuit. The magnetic and electric field distributions [Tang *et al.* (2017)] of the p^{th} *TE* mode in R_1 and R_2 are expressed as, respectively,

$$\left.\begin{aligned} H_{z1\_p} &= \mathrm{Re}\left\{A_p(z)\,\zeta_{1\_p}(r,\varphi)e^{j\omega_p t}\right\} \\ H_{z2\_p} &= \mathrm{Re}\left\{A_p(z)\zeta_{2\_p}(r,\varphi)e^{j\omega_p t}\right\} \end{aligned}\right\} \tag{2.30}$$

$$\left.\begin{aligned} E_{\perp 1\_p} &= A_p(z)\frac{j\omega\mu}{k_{1\_p}^2-k_z^2}\mathrm{Re}\left\{\vec{e}_z\times\nabla_\perp\zeta_{1\_p}(r,\varphi)e^{j\omega_p t}\right\} \\ E_{\perp 2\_p} &= A_p(z)\frac{j\omega\mu}{k_{2\_p}^2-k_z^2}\mathrm{Re}\left\{\vec{e}_z\times\nabla_\perp\zeta_{2\_p}(r,\varphi)e^{j\omega_p t}\right\} \end{aligned}\right\} \tag{2.31}$$

where, $A_p(z)$ is the axial field distribution, $k_{1\_p}^2=\omega_p^2\,\varepsilon_1\,\mu_1$, and $k_{2\_p}^2=\omega_p^2\,\varepsilon_2\,\mu_2$ are the

axial wave numbers of the p^{th} mode in R_1 and R_2, respectively. The angular frequency of the p^{th} mode is ω_p. The function $\zeta_{1\_p}(r,\varphi) = J_{m_p}(k_{\perp 1\_p} r) e^{-im_p \varphi}$ and $\zeta_{2\_p}(r,\varphi) = \left[\alpha J_{m_p}(k_{\perp 2\_p} r) + \beta N_{m_p}(k_{\perp 2\_p} r) \right] e^{-im_p \varphi}$ are the transverse field distribution function in R_1 and R_2, respectively, where, $k_{\perp 1\_p}$ and $k_{\perp 2\_p}$ are the transverse wave number of the p^{th} mode, m is the order of Bessel function, $J_{m_p}(k_{\perp 2\_p} r)$ and $N_{m_p}(k_{\perp 2\_p} r)$ are the Bessel functions of 1st and 2nd kind, respectively, $\alpha = J_{m_p}(k_{\perp 2\_p} r) N'_{m_p}(k_{\perp 2\_p} r) / P(k_{\perp 2\_p} r_w)$, and $\beta = -J_{m_p}(k_{\perp 2\_p} r) J'_{m_p}(k_{\perp 2\_p} r) / P(k_{\perp 2\_p} r_w)$ are constants. Assuming that more than one mode exists simultaneously, the total axial magnetic field component is expressed based on the superposition of various modes,

$$H_{z1} = \sum_p H_{z1\_p} \qquad \text{and} \qquad H_{z2} = \sum_p H_{z2\_p} \tag{2.32}$$

Considering that the electron beam is modeled by N macro particles, the current density distribution $\vec{J}_\perp$ is assumed to be

$$\vec{J}_\perp = -\frac{2\pi |I_0|}{\omega_l} \sum_{i=1}^{N} W_i \frac{1}{r_i} \delta(r - r_i)\, \delta(\varphi - \varphi_i)\, \delta(t - t_i) \frac{\vec{\beta}_i}{\beta_{zi}} \tag{2.33}$$

where, W_i is the weight factor [20], which can be defined as $\sum_i^N W_i = 1$ and N represents the total number of electrons.

The wave equation in the presence of an electron beam can be expressed as,

$$\sum_p \left(\nabla^2 H_{z\_p} + k_z^2 H_{z\_p} \right) = -\left(\nabla \times J \right)_z , \tag{2.34}$$

Using identity $\nabla^2 = \nabla_\perp^2 + \partial^2 / \partial z^2$ and $\nabla_\perp^2 \zeta_p = -k_{\perp\_p}^2 \zeta_p$, wave equation can be given as,

$$\sum_p \mathrm{Re}\left\{ \left(\frac{\partial^2 A_p(z)}{\partial z^2} \zeta_p + A_p(z)\, \nabla_\perp^2 \zeta_p + k_p^2 A_p(z)\, \zeta_p \right) e^{i\omega_p t} \right\} = -(\nabla \times J)_z$$

$$\sum_p \mathrm{Re}\left(\frac{\partial^2}{\partial z^2}+k_{z\_p}^2\right)A_p(z)\zeta_p e^{i\,\omega_k t}=-(\nabla\times J)_z, \tag{2.35}$$

after multiplying by $\zeta_l^* e^{-i\omega_l t}$ in both sides of equation (2.35), and following the integral $\int_0^{2\pi/\omega_l}\int_0^{r_w}\int_0^{2\pi}\langle\ \rangle\, d\varphi\, r dr\, dt,$ the real part of left side of equation (2.35) is given as,

$$\frac{1}{2}\int_0^{\frac{2\pi}{\omega_l}}\int_0^{r_w}\int_0^{2\pi}\sum_p\left\{\left(\frac{d^2}{dz^2}+k_{z\_p}^2\right)\times\begin{bmatrix}A_p(z)\,\zeta_p\,\zeta_l^* e^{-i(\omega_p-\omega_l)t}\\ +A_p^*(z)\,\zeta_p^*\,\zeta_l^* e^{-i(\omega_p+\omega_l)t}\end{bmatrix}\right\}\times\, d\varphi\, r\, dr\, dt \tag{2.36}$$

Using the orthogonal property of ζ_p and ζ_l, the term,

$$\frac{1}{2}\int_0^{\frac{2\pi}{\omega_l}}\int_0^{r_w}\int_0^{2\pi}\begin{Bmatrix}A_p(z)\zeta_p\zeta_l^*\\ +A_p^*(z)\zeta_p^*\zeta_l^* e^{-2i\omega_l t}\end{Bmatrix}\times d\varphi\, r\, dr\, dt=0,\qquad \text{for } p\neq l \tag{2.37}$$

for $p = l$, geometry factor is defined as [4] $G_{mn\_p}=G_1+G_2$,

$$\begin{aligned}G_{mn\_p}=\frac{1}{2}\int_0^{\frac{2\pi}{\omega_p}}dt\iint_{R_1+R_2}\begin{Bmatrix}A_p(z)\zeta_p\zeta_l^*+\\ A_p^*(z)\zeta_p^*\zeta_l^* e^{-2i\omega_l t}\end{Bmatrix}\times d\varphi dr dr\iint_{R_1}\left|\frac{j\omega_k\mu_1}{k_{1\_p}^2-k_{z\_k}^2}\left[\vec{e}_z\times\nabla_\perp\zeta_{1\_p}(r,\varphi)\right]\right|^2\\ \times d\varphi\, r\, dr+\iint_{R_2}\left|\frac{j\omega_k\mu_2}{k_{2\_p}^2-k_{z\_k}^2}\left[\vec{e}_z\times\nabla_\perp\zeta_{2\_p}(r,\varphi)\right]\right|^2\times d\varphi\, r\, dr\end{aligned} \tag{2.38}$$

where, G_1 and G_2 represent geometry factors for region R_1 and R_2, respectively. Using equations (2.37) and (2.38) into equation (2.35), field equation can be written as,

$$\begin{aligned}&\left(\frac{\partial^2}{\partial z^2}+k_{zp}^2\right)A_p(z)=\left(j\,2\pi\left|I_0\right|\mu_1/G_{mn\_p}\right)\times\left(\omega_l/2\pi\right)\\ &\int_0^{\frac{2\pi}{\omega_l}}\int_0^{r_w}\int_0^{2\pi}\left\langle\sum_{i=1}^{N}W_i\frac{1}{r_i}\delta(r-r_i)\,\delta(\varphi-\varphi_i)\,\delta(t-t_i)\,\frac{\vec{\beta}_i}{\beta_{zi}}\zeta_l^*\right\rangle\times d\varphi\, r dr\, dt\end{aligned} \tag{2.39}$$

where, $\zeta_l^*=J_{sl}(k_{\perp l}r_L)\,J_{ml-sl}(k_{\perp l}r_c)\times e^{i\,(m_l-s_l)\,\phi_c+i s_l\theta}$.

2.4.2. Wave Dynamics in Nonlinear (Unloaded) Section

The unloaded section of the waveguide is a simple metal waveguide, where the loss is negligible. Hence, the geometry factor reduces to $G = G_1$ and can be expressed as

$G_1 = \pi r_w^2 \left[1-\left(m^2 / x_{m_p n_p}^2\right)\right] J_m^2(x_{m_p n_p})$. Now, the field evolving equation in the unloaded section can be written as [19],

$$\left(\frac{d^2}{dz^2}+k_{zl}^2\right)A_l(z) = \frac{-2|I_b|k_{\perp 1}}{\pi r_w^2\left[1-\frac{m^2}{x_{m_p n_p}^2}\right]J_m^2(x_{m_p n_p})} \times \sum_{i=1}^{N} W_i \frac{\upsilon_{\perp i}}{\upsilon_{zi}}\left[\sum_{s=-\infty}^{\infty} J'_{sl}(k_{\perp l} r_{Li}) J_{ml-sl}(k_{\perp l} r_{ci}) e^{-j\Lambda_i}\right] \tag{2.40}$$

where, $\Lambda_i = \omega_l t_i - (m_l - s_l)\phi_{ci} - s_l \theta_i$ is the phase distribution.

2.4.3. Electron Beam Dynamics in Interaction Waveguide

The self-consistent electron beam-wave interaction can be specified by the equation of electron motion. In the presence of three forces: (i) axial DC magnetic field, (ii) influence of high-frequency field, and (iii) transverse DC magnetic field, respectively, the equation of electron momentum can be expressed by [Du and Liu (2014), Tang *et al.* (2017)],

$$\frac{d\vec{p}}{dt} = -e\vec{v}\times\vec{B}_0 - e(\vec{E}+\vec{v}\times\vec{B}) + e\vec{B}_0 g(\vec{v}\times\vec{r}) \tag{2.41}$$

where, $g = \left(1/2\vec{B}_0\right)\left(d\vec{B}_0/dz\right)$, $\vec{E}$ and $\vec{B}$ are the electric and magnetic fields, respectively, $\vec{p}$ and $\vec{v}$ are the momentum and velocity of electrons, respectively, and γ is the relativistic factor. Based on this, the equation of electron motion describing the axial momentum (p_z), transverse momentum (p_t), rotation angle (θ), guiding center radius (r_c), and guiding center angle (ϕ_c) are expressed through (2.42a) — (2.42e), respectively [Tang *et al.* (2017)].

$$\frac{dp_z}{dz} = -m_e cg\frac{\beta_t^2}{\beta_z} + \frac{e\mu_0 v_t}{v_z}\mathrm{Re}\left\{\sum_p \frac{1}{k_{t\_p}} A_p'(z) J_{s_p}'\left(k_{t\_p} r_L\right) J_{m_p - s_p}\left(k_{t\_p} r_c\right) e^{i\Lambda}\right\}, \tag{2.42a}$$

$$\frac{dp_t}{dz} = -m_e cg\beta_t + \frac{e\mu_0}{v_z}\mathrm{Re}\left\{\sum_p \frac{1}{k_{t\_p}}\left(i\omega_p A_p(z) + \upsilon_z A_p'(z)\right) \times J_{s_p}'\left(k_{t\_p} r_L\right) J_{m_p - s_p}\left(k_{t\_p} r_c\right) e^{i\Lambda}\right\}, \tag{2.42b}$$

$$p_t\left(\frac{d\theta}{dz} - \frac{eB_0}{p_z}\right) = -\frac{e\mu_0}{v_z} \times \mathrm{Re}\left\{\begin{array}{l}\sum_p \frac{1}{k_{t\_p}^2}\left(\frac{s_p\omega_p}{r_L} f_p(z) - k_{t\_p}^2 \upsilon_t A_p(z) - \frac{is_p}{r_L}\upsilon_z A_p'(z)\right) \\ \times J_{s_p}\left(k_{t\_p} r_L\right) J_{m_p - s_p}\left(k_{t\_p} r_c\right) e^{i\Lambda}\end{array}\right\}, \tag{2.42c}$$

$$\frac{dr_c}{dz} = -gr_c + \frac{\mu_0}{B_0 v_z}\sum_l \left\{\begin{array}{l}\frac{1}{k_{t\_p}} J_{s_p}\left(k_{t\_p} r_L\right) J_{m_p - s_p}'\left(k_{t\_p} r_c\right).\left[\mathrm{Re}\left(i\omega_p A_p(z) + \upsilon_z A_p'(z)\right)\right] \times e^{i\Lambda} \\ -\left[\begin{array}{l} J_{s_p - 1}\left(k_{tl} r_L\right) J_{m_p - s_p + 1}\left(k_{t\_p} r_c\right) \\ -J_{s_p + 1}\left(k_{t\_p} r_L\right) J_{m_p - s_p - 1}\left(k_{t\_p} r_c\right)\end{array}\right] \times \mathrm{Im}\left(\frac{1}{2}\upsilon_t A_p(z) e^{i\Lambda}\right)\end{array}\right\} \tag{2.42d}$$

$$r_c\frac{d\phi_c}{dz} = \frac{\mu_0}{B_0 v_z}\sum_l \left\{\begin{array}{l}\frac{1}{k_{tl}^2}\frac{m_p - s_p}{r_c} J_{s_p}\left(k_{t\_p} r_L\right) J_{m_l - s_p}\left(k_{t\_p} r_c\right).\left[\mathrm{Im}\left(i\omega_p A_p(z) + \upsilon_z A_p'(z)\right)\right] \times e^{i\Lambda} \\ -\left[\begin{array}{l} J_{s_p\text{-}1}\left(k_{t\_p} r_L\right) J_{m_p\text{-}s_p + 1}\left(k_{t\_p} r_c\right) \\ +J_{s_p + 1}\left(k_{t\_p} r_L\right) J_{m_p\text{-}s_p\text{-}1}\left(k_{t\_p} r_c\right)\end{array}\right] \times \mathrm{Re}\left(\frac{1}{2}\upsilon_t A_p(z) e^{i\Lambda}\right)\end{array}\right\} \tag{2.42e}$$

2.5. Benchmarking with Experimental Gyro-TWT

The steady-state multimode nonlinear code for the lossy dielectric loaded gyro-TWT has been benchmarked with the experimental gyro-TWT reported by Song *et al.* [Song *et al.* (2004)]. The initial 12 cm length (linear section) of RF interaction waveguide circuit is heavily loaded with a lossy dielectric with resistivity of 70,000 times copper resistivity to suppress the gyro-BWOs. The final 2.5cm (nonlinear section) is unloaded to avoid the damping of the operating wave. A total loss of ~90dB loss in lossy linear section is predicted by the cold test simulation. The electron beam parameter used for the nonlinear simulation is 100kV and 5A with an axial velocity spread of 5%. The detailed parameter list is shown in the Table 2.1. The multimode wave particle interaction behavior of the gyro-TWT is analyzed using the multimode nonlinear code. Figure 2 shows the growth of the operating TE_{01} mode along with

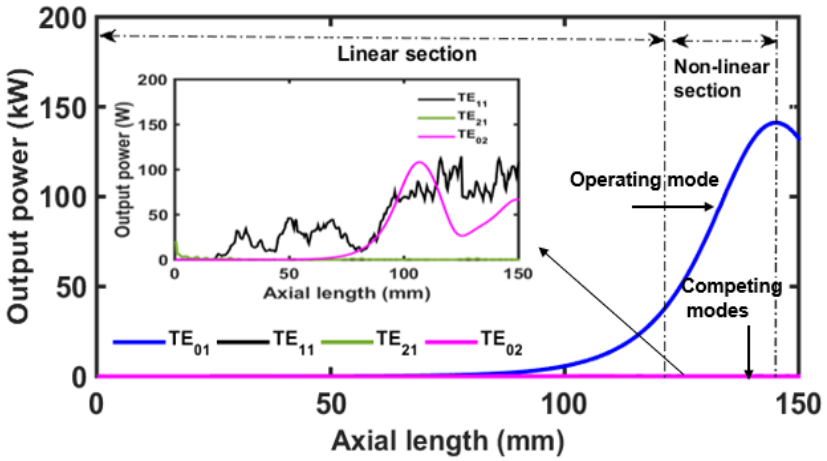

Figure. 2.2 Growth of operating TE_{01} mode along with competing modes (inset) in both linear and non-linear sections.

Table 2.1: Parameters List For W-Band Gyro-TWT [Song *et al.* (2004)]

Parameters	Values
Operating Mode	TE_{01}
Lossy wall resistivity	$70{,}000\rho_{Cu}$
Beam Voltage (V)	100 kV
Beam Current (I)	5 A
Guiding Center radius (r_g)	0.9648 mm
Larmor radius (r_L)	0.22 mm
Velocity ratio (α)	5 %
DC Magnetic Field, B_0	3.56 T
Total Lossy section length (L_1)	12.0 cm
Copper circuit length (L_2)	2.5 cm

competing modes in the interaction circuit. The figure shows that strength of the wave is weakened in the lossy section due to the attenuation and it gets maximum amplification in the unloaded section. The lossy linear section provides heavy attenuation to competing modes, including ~6.5 dB / cm TE_{11} mode (at ~67 GHz), ~11.30 dB /cm to TE_{21} mode (77 GHz), and ~18.50 dB /cm to TE_{02} mode (at 166.5 GHz), as compared to ~7.5 dB /cm (~90dB / 12cm) to the operating TE_{01} mode at 92 GHz. The RF power developed in the desired operating TE_{01} mode is ~145 kW as shown in Figure 2.2, the power in all other competing modes including TE_{11}, TE_{21}, and TE_{02} modes is ~100W,

~1W, and ~100W, respectively. The obtained simulation results are also compared using 3D PIC simulation code, which will be discussed in Chapter 3.

2.6. Concluding Remarks

In this chapter the fundamental theory of dielectric loaded waveguide interaction structure for gyro-TWT amplifier has been revisited and understood. The linear and single mode nonlinear theory for gyro-TWT with dielectric waveguide interaction circuit has been studied. Since the single mode analysis fails to give the mutual effect of operating and oscillating mode, a multimode nonlinear analysis has been presented and benchmarked with an experimental W-band gyro-TWT [Song *et al.* (2004)]. In the next chapter, 3D PIC simulation investigation of uniform dielectric loaded interaction structure for W-band gyro-TWT amplifier will be discuss along with design and simulation of various subassemblies of gyro-TWT amplifier.